Published in final edited form as:
J Comp Neurol. 2010 July 1; 518(13): 2554–2569. doi:10.1002/cne.22352.

Expression of BK-Type Calcium-Activated Potassium Channel Splice Variants During Chick Cochlear Development

Jung-Min Kim[1,2], **Ryan Beyer**[1], **Marti Morales**[1], **Stephanie Chen**[1], **Li Qian Liu**[1], and **R. Keith Duncan**[1,*]

[1]Kresge Hearing Research Institute, University of Michigan, Ann Arbor, Michigan 48109

[2]Medical Sciences, Boston University School of Medicine, Boston, Massachusetts 02215

Abstract

The appearance of large-conductance, calcium-activated potassium (BK) current is a hallmark of functional maturation in auditory hair cells. Acquisition of this fast-activating current enables high-frequency, graded receptor potentials in all vertebrates and an electrical tuning mechanism in nonmammals. The gene encoding BK α subunits is highly alternatively spliced, and the resulting variations in channel isoforms may contribute to functional diversity at the onset of hearing. We examined the tissue specificity of nine BK α alternative exons and investigated changes in expression during chick cochlear development using quantitative polymerase chain reaction (qPCR). Each alternative was widely expressed in several tissues except for an insert near the C-terminus Ca^{2+} sensing domain, which appeared brain-specific. The only alternative form in the membrane-bound core of the channel was expressed in brain and muscle but was undetected in cochlea. Of the remaining variants, three increased in expression prior to the onset of hearing and acquisition of BK currents. These three variants cause decreased Ca^{2+} sensitivity or increased intracellular retention, traits that would not easily explain the advent of calcium-sensitive currents at embryonic day (E)18–19. Expression levels of other variants were mature and stable by E15, days before currents were acquired. Surface expression of C-terminal isoforms was examined using patch-clamp electrophysiology and immunocytochemistry. C-terminal variants that exhibit robust surface expression appeared in the membrane at E18, even though transcripts were unchanged during development starting from E12. These results indicate that delays in protein synthesis and trafficking/scaffolding of channel subunits underlie the late acquisition of BK currents in cochlear hair cells.

INDEXING TERMS

Maxi-K; BKCa; basilar papilla; hair cell; alternative exon

The BK-type potassium channel is an effective regulator of membrane excitability by combining an exceptionally large conductance, up to 50 times that of other K^+ channels (Hille, 2001), with dual sensitivity to intracellular calcium and membrane potential (Latorre et al., 1989). The versatility of this channel is further expanded by an array of interaction partners (Lu et al., 2006; Salkoff et al., 2006) and extensive alternative splicing of the gene encoding the pore-forming BK α subunits (*KCNMA1*; Slo1). These traits lead to diverse

*CORRESPONDENCE TO: R. Keith Duncan, PhD, Kresge Hearing Research Institute, University of Michigan, 5323A Medical Science Building I, 1150 W. Medical Center Drive, Ann Arbor, MI 48109-5616. rkduncan@umich.edu.
The first two authors contributed equally.

Additional supporting information may be found in the online version of this article.

physiological roles in neuronal excitability, smooth muscle tone, hormone release, and sound processing. In the cochlea, BK channels play a major role in shaping the hair cell receptor potential (Housley et al., 2006). The large current density and rapid kinetics enable fast repolarization during sound stimulation and contribute to high-fidelity temporal processing in the auditory periphery (Oliver et al., 2006). Additionally, in nonmammalian vertebrate cochleae the close proximity of BK channels and voltage-gated calcium channels facilitates an intrinsic electrical tuning mechanism (Roberts et al., 1990; Fettiplace and Fuchs, 1999). Systematic changes in BK kinetics have been described at the single-channel level along the auditory epithelia of turtles (Art et al., 1995) and chicks (Duncan and Fuchs, 2003). Therefore, variations in BK channel structure-function is a primary determinant of frequency selectivity in these animals (Fettiplace and Fuchs, 1999).

The sudden appearance of BK currents at the onset of hearing in both mammals and nonmammals underscores the importance of these channels in hair cell function (Fuchs and Sokolowski, 1990; Marcotti et al., 2003). For example, in chicks hearing thresholds dramatically improve around embryonic day 18 (E18) (Saunders et al., 1973), coincident with the acquisition of calcium-sensitive BK currents (Fuchs and Sokolowski, 1990). Within 1 to 2 days, current levels are mature, marking a transition in hair cell physiology from an immature spiking cell to a graded receptor cell. These events take place days-to-weeks after terminal hair cell differentiation and after the acquisition of other voltage-sensitive and mechanically gated channels essential to hair cell physiology (Fettiplace and Fuchs, 1999; Housley et al., 2006). The molecular mechanisms that regulate BK behavior in the cochlea remain unclear, but alternative splicing has been proposed as a central means for diversifying BK properties in the cochleae of mammals (Langer et al., 2003; Beisel et al., 2007), turtles (Jones et al., 1998), and chicks (Navaratnam et al., 1997; Rosenblatt et al., 1997). In this study, alternative splicing was investigated as a means for controlling the late-stage appearance of BK function in chick cochlear hair cells.

Eight splice sites and over 10 alternative exons have been identified in the chick cochlea, potentially giving rise to hundreds of distinct channel configurations (Fettiplace and Fuchs, 1999). While the functional consequences of most variants are still to be examined, alternative splicing has been shown to impact channel biophysics (Lagrutta et al., 1994; Jones et al., 1999; Ha et al., 2000; Ramanathan et al., 2000), surface expression (Zarei et al., 2004; Kim et al., 2007; Ma et al., 2007), and interaction with various modulators (Kim et al., 2008; Pietrzykowski et al., 2008). We hypothesized that changes in splice patterns regulate the sudden acquisition of BK current in the chick cochlea. Contrary to this hypothesis, our results clearly show that changes in overall transcript abundance and changes in the abundance of specific splice forms cannot explain the sudden development of functional current.

MATERIALS AND METHODS

Tissue preparation

All animal procedures were approved by the University of Michigan Committee on Use and Care of Animals. Tissue samples were obtained from white leghorn chickens (*Gallus gallus*) at three embryonic ages (E12, E15, and E18) and from posthatch (PH) animals 7 to 14 days after hatching. Embryonated eggs were obtained from the Michigan State University Poultry Teaching and Research Center and maintained at 40°C in a humidity-controlled incubator. Embryonic age was determined according to the morphological atlas of Hamburger and Hamilton (1951). Posthatch animals were anesthetized with ketamine/ xylazine (≈40 mg/kg and 10 mg/kg, respectively, via intramuscular injection) prior to euthanasia by rapid decapitation. Cochlear samples were extracted and pretreated with protease (0.01–0.1%, type XXIV, Sigma, St. Louis, MO) in extracellular fluid (ECF) (in mM: 154 NaCl, 6 KCl, 5

$CaCl_2$, 2 $MgCl_2$, 5 HEPES, at pH 7.4). The overlying tegmentum vasculosum and the supporting cells lying on the margins of the basilar papilla were removed and the sensory epithelia dissected free for further analysis. In this way, samples were enriched with hair cells and devoid of sensory ganglion and vascularized structures, both of which express the gene targets of interest.

Real-time and routine polymerase chain reaction (PCR)

Tissue samples were obtained under RNase free conditions. Intact organs were isolated, washed with ECF, and flash-frozen on dry ice. Samples included whole cerebellum, chick fast skeletal muscle from the breast, proventricular smooth muscle, cardiac muscle, whole cochlear ducts, and liver. Bulk tissue samples were mechanically homogenized (Tissue Tearor, BioSpec Products, Bartlesville, OK), and total RNA was extracted in Trizol (Invitrogen, La Jolla, CA) followed by an RNA cleanup procedure (RNeasy Mini Kit, Qiagen, Chatsworth, CA). Six to 12 sensory epithelia were pooled because of the low yield of RNA from this restricted tissue. Saline from each dissection was collected to determine whether RNA from disrupted accessory tissues confounded the data. For basilar papilla and saline samples, RNA was extracted using an RNeasy Micro Kit (Qiagen). The quantity of RNA was determined by spectrophotometry (NanoDrop 1000, Thermo Scientific, Waltham, MA) and the quality of RNA samples was determined by an Agilent 2100 Bioanalyzer (Agilent Technologies, Palo Alto, CA) to ensure the integrity of the starting material (RIN > 8). Total RNA was reverse-transcribed using Superscript III (Invitrogen).

Several samples in random combinations of age or tissue type were analyzed in parallel to avoid bias. At least three biological repeats from different animals were obtained for each measurement. Reverse transcriptase (RT) was excluded from at least one sample per experimental run as a no-RT control to test for genomic DNA or expression plasmid contamination. Quantitative real-time PCR (qPCR) was performed on the cDNA, saline controls, and no-RT controls using custom TaqMan fluorogenic probes (Applied Biosystems, Foster City, CA). The amplification of target gene products was detected with an ABI Prism 7900HT Sequence Detection System or an ABI StepOne Real-time PCR system (Applied Biosystems). Comparisons were made using the ΔΔCT method of relative quantification (Livak and Schmittgen, 2001). For each experiment, a line was placed in the log-linear phase of amplification to determine the threshold cycle number (CT). Reactions were performed in triplicate and averaged to determine the mean CT value. Data were discarded if the standard deviation for triplicate mean was greater than 0.5. In some cases for CT values above 36, this criterion was relaxed since variance increases substantially for low-copy amplification in this CT range. To determine relative changes in expression level, the CT for a gene of interest was normalized against a reference such that $\Delta CT = CT_{\text{gene of interest}} - CT_{\text{reference}}$. Next, the ΔCT values for two groups were compared (ΔΔCT) and used to determine the fold-change in the gene of interest ($2^{-\Delta\Delta CT}$).

Routine PCR reactions were performed on a Mastercycler Gradient (Eppendorf, Hamburg, Germany) using Platinum Taq DNA polymerase. To improve the yield of small PCR products, reactions included 5% dimethyl sulfoxide. Custom primers (Invitrogen) were generated using sequences included in TaqMan assays or designed using Primer3 (http://frodo.wi.mit.edu/). PCR products were separated on a 3% agarose gel, stained with ethidium bromide, and digitized with a FluorChem SP imaging system (Alpha Innotech, San Leandro, CA).

Alternative splicing nomenclature and TaqMan probe design

In this article the term “variant” will be reserved for a full-length mRNA or protein sequence containing a specific subset of constitutive and facultative exons. “Alternative exon” will

refer to nonobligatory inserts, 5′ or 3′ extensions of obligatory exons, and mutually exclusive exons. Thus, unique splice variants arise from any combination of alternative exons at individual alternative splice junctions. Establishing a unified nomenclature for these variants is a daunting task. As a result, naming schemes for *KCNMA1* splice forms abound (Tseng-Crank et al., 1994; Fettiplace and Fuchs, 1999; Yu et al., 2006; Beisel et al., 2007; Fodor and Aldrich, 2009). Unfortunately, none of these schemes capture all of the alternative exons reported in the literature (for example, see Korovkina et al., 2001; Zarei et al., 2001). While 28 constitutive exons are highly conserved across species, the number and position of alternative splice events is diverse (Fodor and Aldrich, 2009). The problem is compounded by the lack of a comprehensive single-gene library of splice forms in public databases. Therefore, international guidelines for the naming of alternative splice forms cannot be applied, since these rely on unique accession numbers for full-length variants (International Committee on Standardized Genetic Nomenclature for Mice, http://www.informatics.jax.org/mgihome/nomen/gene.shtml). In the absence of a universally accepted nomenclature for *KCNMA1*, we will refer to alternative exons according to splice site and the amino acid products encoded at that site.

Our study focused on alternative exons previously identified by library screening and PCR amplification using chick cochlea (Rosenblatt et al., 1997; Navaratnam et al., 1997; Ramanathan et al., 2000). Exon structure is illustrated in Fig. 1A. The numbering of splice sites follows the scheme of Fettiplace and Fuchs (1999). Alternative exons are illustrated at splice sites X1 through X7. Site X0 has been omitted since splice variation reported at the 5′ end of the sequence (Rosenblatt et al., 1997) appears to be a cloning artifact (Beisel et al., 2007). Amino acid sequences corresponding to individual alternative exons and combinations at X4 and X7 are shown in Fig. 1B. The topology of the BK α subunit is shown in Fig. 1C and the relative position of the alternative splice sites indicated (*). All but one splice site occurs in the intracellular portion of the protein.

Alternatives at each splice site were named according to the splice site and number of incorporated amino acids. For instance, the eight amino-acid insert at site X1 is referred to as $\alpha_{X1}(8)$. Illustrations in Table 1 depict the orientation and approximate position of primers and probes for each alternative exon or combination of exons. Primer/probe combinations also were developed for a housekeeping gene (the small ribosomal subunit, S16) and a nonvariant-specific BK reporter (α_X). The probe for α_X targeted an exon–exon boundary with no reported alternative exons, and primers for this probe were positioned in the constitutive exons spanning this boundary. As such, this probe reflected the amplification of all BK α transcripts, regardless of alternative exons at other splice junctions. All TaqMan assays were designed in conjunction with Applied Biosystems using published sequences or those derived from the chicken genome. In all cases, probes crossed splice junctions, reducing the influence of genomic DNA, if present.

HEK293 culture and transfection

Transient expression of full-length chicken BK isoforms was accomplished as described previously (Duncan, 2005). Briefly, HEK293T cells (ATCC, American TypeCulture Collection, Rockville, MD) were maintained in growth medium consisting of high-glucose DMEM (Invitrogen) supplemented by 10% defined fetal bovine serum (Hyclone, Logan, UT) and 1% penicillin/streptomycin (Invitrogen). The cells were cultured in 5% CO_2 at 37°C. For transfection experiments, cells were grown on glass coverslips and transiently transfected using Lipofectamine 2000. Plasmid constructs were derived from a clone of the full-length chicken BK α subunit (*cslo1*) packaged in a mammalian expression vector (pcDNA3.1) (Jiang et al., 1997). Gene inserts included the cslo1 clone ending in QEDRL or an alternative variant ending in VEDEC (gift from Dr. Paul A. Fuchs, Johns Hopkins University, Baltimore, MD), corresponding to $\alpha_{X7}(7)$ and $\alpha_{X7}(60)$, respectively.

Transfections included pEGFPLuc (BD Biosciences ClonTech, San Jose, CA) for fluorescence detection of transfected cells.

Immunohistochemistry

Isolated hair cells were prepared for immunohistochemistry by mechanically dissociating the basilar papilla (one per slide). Cells were dispersed into ECF on Superfrost Plus slides (Fisher Scientific, Pittsburgh, PA) within a rubber-cement barrier. Cells were fixed with 2% parafor-maldehyde (PFA) for 30 minutes, permeabilized with 0.1% Triton X-100 for 15 minutes, blocked with 10% normal donkey serum in phosphate-buffered saline (PBS, pH 7.4) for 1 hour, and incubated with primary antibodies overnight at 4°C. Custom antibodies to C-terminus epitopes (gifts of Dr. Stuart Dryer, University of Houston, Houston, TX) were diluted to a concentration of 1:4,000 in PBS. These affinity-purified polyclonal antibodies were raised against synthetic peptides corresponding to mammalian isoforms. Anti-QEERL was derived from the immunizing peptide THMRPNRTKTRDSREKQKYVQEERL (avian isoform ends in QEDRL) and specifically detects $\alpha_{X7}(7)$. Anti-VEDEC was derived from the immunizing peptide ANQINQYKSTSSLIPPIREVEDEC (avian isoform ends in VEDEC) and specifically detects $\alpha_{X7}(60)$. Previous work confirmed the specificity of these antibodies using Western blot analysis on chick ciliary ganglion lysates and total protein from HEK293 cells transiently transfected with mammalian isoforms (Kim et al., 2007). No signal was detected in untransfected HEK293 cells. Bands matching the predicted size of the BK α subunit (≈ 130 kDa) were observed, along with heavier bands corresponding to multimers. No additional nonspecific bands were detected. After incubation with our preparations, cells were washed extensively followed by exposure to highly cross-absorbed donkey antirabbit secondary antibody (Alexa-Fluor 594; Invitrogen) at 1:500 in PBS. In some cases cells were counterstained with Hoechst 33242 and Alexa-Fluor 488-phalloidin to visualize the cell nucleus and hair bundle, respectively. HEK293 cells were treated similarly with slight variations in permeabilization conditions (i.e., duration and inclusion with antibody diluents) and block (Universal Blocking Reagent; BioGenex, San Ramon, CA). Control preparations, in which the primary antibody was omitted, were imaged under comparable exposure conditions to test for specificity of the secondary label. Epifluorescence images were obtained using a Leica DM LB fluorescence microscope with a cooled-CCD color digital camera (MicroPublisher, Q Imaging). Confocal images were obtained with an Olympus Fluoview FV500. Postprocessing of original images was limited to cropping and rescaling. Overlays for merged fluorescence and differential interference contrast (DIC) images were created in Adobe Photoshop CS2 (San Jose, CA). Supporting movies were generated using Imaris (6.2.1) (Bitplane).

Electrophysiology

Voltage-clamp recordings were made from inside-out patches from transiently transfected HEK293T cells as described previously (Duncan, 2005). Briefly, recordings were obtained from cells 24–48 hours after transfection. Identical solutions were presented to both sides of the excised patch, each consisting of 142 mM KCl, 0.5 mM $MgCl_2$, 5 mM HEPES, 2 mM Br_2BAPTA, and enough $CaCl_2$ to reach a free Ca^{2+} concentration of 1 μM. Calcium concentration was calibrated using a calcium-sensitive electrode (World Precision Instruments, New Haven, CT). Recordings were made with a Multiclamp 700B amplifier, Digidata 1440A digitizer, and the pClamp 10.0 software suite (Molecular Devices, Palo Alto, CA). Up to 20 stimulus presentations were averaged to produce ensemble currents from patches with ≈2–200 channels. Capacitance and leak currents were subtracted offline. Conductance-voltage (G-V) curves were constructed from steady-state currents and fitted with a first-order Boltzmann function: $G = G_{max} / (1 + e^{-(V_{1/2} - V) / V_e})$, where G_{max} is the maximum conductance level, $V_{1/2}$ is the half-activating voltage, and V_e is the Boltzmann slope. All recordings were made at room temperature (22–25°C).

Statistical analyses

Averaged values were reported as means ± one standard error of the mean. A Student's *t*-test was used when comparing differences in mean values between two groups. A one-way analysis of variance (ANOVA) was used to determine the significance of gene expression changes during cochlear development. In both cases, significant differences were indicated by $P < 0.05$.

RESULTS

Several alternative exons have been identified by library screening and PCR amplification using chick cochlear cDNA (Rosenblatt et al., 1997; Navaratnam et al., 1997; Ramanathan et al., 2000). Although additional alternatives have been reported in other species and other tissues (Fodor and Aldrich, 2009), we focused attention on those splice forms that may contribute to the diversity of BK function in chick hair cells. The relative size, position, and coding sequence of these exons are illustrated in Fig. 1. TaqMan assays were developed to assess the expression levels of these exons, and in some cases combination of exons, according to the schematics in Table 1. Exon extension at site X5 was excluded from this study since a recent report noted the absence of alternative splicing at this site in nonmammalian species (Beisel et al., 2007).

Primer specificity was tested using routine PCR to ensure that a single amplicon containing the probe sequence was produced. With one exception, the TaqMan primers produced amplicons of the correct size, indicating high specificity for the intended gene products (data not shown). The single exception occurred at X2, where primers produced one product of the expected size and a second ≈100 bp larger. The extraneous product was sequenced, and no homology with the TaqMan probe sequence was found. The amplification efficiency of the TaqMan probes was assessed using serial dilutions of chick brain cDNA (Supporting Fig. 1). The dilution curves for all probes were linear with $R^2 \geq 0.99$, and their slopes varied between −1.0 and −1.1, satisfying both the linearity and efficiency requirements for relative gene expression assays (Wong and Medrano, 2005).

Tissue distribution

The overall expression of BK transcripts was lower in all tissues examined compared to that in the brain (Fig. 2A) ($P < 0.05$). This result reflected the increased proportion of electrically excitable cells in brain compared with other tissues. To identify tissue-specificity with regard to particular variants, probes targeting alternative exons were normalized to α_X to indicate the prevalence of a variant among all α transcripts (Fig. 2B–J). Nearly half of the alternatives tested, $\alpha_{X2}(31)$, $\alpha_{X4}(58+)$, $\alpha_{X7}(7)$, and $\alpha_{X7}(6)$, showed comparable levels of expression among the various tissues, within 10-fold above or below expression levels in chick brain. Only $\alpha_{X7}(7)$ was enriched in all organs compared to brain. Differences were relatively small, but significant ($P < 0.05$). Interestingly, decreases in another exon at the same splice site, $\alpha_{X7}(6)$, mirrored the increases seen in $\alpha_{X7}(7)$, possibly indicating a systematic exchange of variants ending in EMVYR for those ending in QEDRL.

Other alternative exons were expressed in a tissue-specific manner. $\alpha_{X1}(8)$ showed little amplification in basilar papilla and cochlea. For these auditory tissues, real-time amplification curves often fell below the threshold line, even though $\alpha_{X1}(8)$ was easily detected in chick brain. Although copy-number was not systematically measured with our approach, we conclude that $\alpha_{X1}(8)$ was expressed in low abundance in the cochlea. Another probe, $\alpha_{X3}(4+)$, was undetected in some tissues while prevalent in others. This probe targeted the 5′ portion of the alternative exon at site X3, thereby capturing truncated and nontruncated variations of exon 19. Expression of $\alpha_{X3}(4+)$ was below detection levels in

heart and liver, but expression levels were comparable in basilar papilla and brain. In contrast, a probe specific for the nontruncated exon 19 ($\alpha_{X3}(20)$) was readily detected in all tissues. This full-length alternative was expressed 10–100-fold less in all tissues compared with brain. Detection of $\alpha_{X3}(20)$ in heart and liver indicated that this probe was more sensitive than the $\alpha_{X3}(4+)$ probe, since $\alpha_{X3}(20)$ should only capture a subset of X3 variants. This difference in detection limits emphasizes that fluorescence curves that fall below threshold should be interpreted cautiously. Such a result implies low abundance but does not unequivocally mean that mRNAs were absent from the starting material. Two other splice events showed some tissue specificity. The insert at X6 was poorly represented in all tissues compared to brain with the largest disparity occurring between brain and basilar papilla (>2,000-fold decrease). In contrast, the long C-terminus variation at X7 was enriched in auditory tissues and suppressed in other organs, compared with brain.

Developmental changes

BK transcripts were detected as early as E12 (Fig. 3A), as recently described (Li et al., 2009). The gradual and modest increases in BK mRNA levels during development are a stark contrast to the sudden appearance of calcium-sensitive BK currents between E18 and E19 (Fuchs and Sokolowski, 1990). Alternative splicing is a key regulator of BK surface expression, leading to the possibility that splice variation contributes to the trafficking/scaffolding mechanisms regulating BK current at the onset of hearing. Several variants have been identified as dominant-negative, cytoplasmically retentive isoforms. One of these described previously in rat and human includes a novel insert (SV1) located in the cytoplasmic loop between transmembrane domains S0 and S1 (Zarei et al., 2001). A BLASTN search of the chick genome using the full SV1 sequence from human and rat returned no sequences of significant homology. Furthermore, we scanned intronic sequences corresponding to chick *Kcnma1* for the ER-retention motif (CVLF) that resides within SV1 (Zarei et al., 2004). Instances of CVLF occur five times in the three reading frames of intron 2, located between exons coding for the S0-S1 cytoplasmic loop. No other significant homology to SV1 is found in these instances. Nevertheless, we designed primers spanning this intronic sequence to further confirm the absence of SV1. PCR amplification using embryonic and posthatch chick brain cDNA only returned bands corresponding to insertless transcripts (data not shown), leading to the conclusion that SV1/CVLF is absent from chick.

A second cytoplasmically retentive isoform has been described in chick ciliary ganglion (Kim et al., 2007). Variants with the C-terminus alternative exon ending in VEDEC, $\alpha_{X7}(60)$, were previously amplified from the cochleae of chick (Rosenblatt et al., 1997), mouse (Beisel et al., 2007), and rat (Langer et al., 2003). A third alternative exon contains a canonical ER retention sequence (RKR, exon 19 at X3) but has not been described as retentive in BK channel studies (Tseng-Crank et al., 1994; Rosenblatt et al., 1997). It is possible that these and other exons contribute to BK trafficking in the chick cochlea. To assess the developmental changes in various alternative exons, cDNA from basilar papilla at E12, E15, E18, and PH were examined with real-time qPCR, normalizing expression to the total pool of BK α transcripts (α_X) (Fig. 3B).

Throughout development $\alpha_{X1}(8)$ remained undetected, indicating that this alternative exon was low abundant in all age groups. In contrast, $\alpha_{X2}(31)$ transcripts were initially undetected at E12 but readily apparent from E15 onward (Fig. 3B). The proportion of this variant increased almost 10-fold between E15 and PH ($P < 0.05$). To provide some indication of the fold-increase between E12 and PH, we assigned a CT of 40 (i.e., the highest cycle number in the qPCR protocol) to the E12 data and repeated the analysis. The results indicated a more than 100-fold increase in this variant between E12 and PH. Since CTs for undetected samples at E12 were artificially assigned, this 100-fold increase underestimates the true change in expression level over these ages.

The next three splice sites, X3–X5, are located between two homologous domains involved in calcium-dependent gating (RCK1 and RCK2) (Fig. 1). Only inserts at X3 and X4 have been amplified from chick basilar papilla and confirmed by analysis of the chick genome. Of the two probes designed to alternatives at X3, α_{X3}(4+) showed a 19-fold increase at E15 that was maintained in older animals (Fig. 3C), whereas α_{X3}(20) increased only in PH basilar papilla by a mere 2-fold (Fig. 3D). These data suggested that isoforms incorporating SRKR-alone were upregulated at E15 and those containing the nontruncated 20-amino-acid insert were further upregulated in PH animals, though to a lesser degree. A previous study considered expression changes at X4 (Li et al., 2009). The proportion of α_{X4}(58+) changed minimally during development, increasing by 2-fold in posthatch animals compared to E11 embryos.

Inserts at X6 are of interest because of the proximity to the so-called Ca^{2+} bowl (Fig. 1), a key calcium-sensing domain in the BK α subunit. In our tissue distribution study, the expression of α_{X6}(28) was more than 2,000-fold less in PH basilar papilla compared to that in brain. The proportion of this variant remained unchanged during papillary development (Fig. 3E). Therefore, its utilization within the cochlea and its contribution to hair cell physiology appear minimal.

Mutually exclusive splicing at X7 generates at least three different C-termini in chick basilar papilla. Developmental changes in the prevalence of these alternatives are of particular interest because of their known roles in trafficking and surface expression. While α_{X7}(6) and α_{X7}(7) produce plasmalemmal channels, α_{X7}(60) is often retained in endoplasmic reticulum (Kim et al., 2007) or trafficked to mitochondria (Kathiresan et al., 2009). We hypothesized that a switch from α_{X7}(60) to α_{X7}(6) and α_{X7}(7) was responsible for the sudden appearance of BK currents at E18–19 (Fuchs and Sokolowski, 1990). However, the proportional expression of α_{X7}(60) increased from E12 to E15 by 4-fold. This higher level of expression was maintained throughout maturation of the basilar papilla. Developmental changes in the other two variants were insignificant ($P > 0.05$) (Fig. 3F–H).

Overall, only three probes showed statistically reliable changes near the onset of hearing [α_{X2}(31), α_{X3}(4+), and α_{X7}(60)]. In all three cases, the alternatives became more highly represented in the total pool of BK transcripts as the basilar papilla matured. There are no reports on the biophysical consequences of the tandem repeat α_{X2}(31), so it is difficult to predict whether this isoform could play a role in current acquisition at the onset of hearing. The location of this alternative splice event suggests a modest effect on channel conductance rather than a profound effect on membrane density (see Discussion). Variants incorporating the 4-amino-acid insert at X3 are less calcium sensitive (Rosenblatt et al., 1997; Ramanathan et al., 1999), so it is surprising to find that the proportion of this variant increases at a time when highly calcium-sensitive current is measured. The 60-amino-acid alternative at X7 also cannot easily explain the sudden appearance of BK current in development, since this exon can exert a dominant-negative effect on channel surface expression (Kim et al., 2007; Ma et al., 2007; Kathiresan et al., 2009). However, plasmalemmal trafficking of α_{X7}(60) can be stimulated by several cofactors, including nephrin (Kim et al., 2008) and β-neuregulin-1 (Kim et al., 2007). The combined effects of a developmentally regulated chaperone and the upregulation of α_{X7}(60) mRNA at E15 might explain the delay between transcription at E12 and function at E18–19. To test this possibility, we sought to correlate qPCR data with studies of protein expression.

Expression of C-terminus variants

Evidence for the reduced surface expression of α_{X7}(60) was obtained previously with biotinylation assays, immunolocalization, and whole-cell electrophysiology using tagged mammalian isoforms in heterologous expression systems (Kim et al., 2007; Ma et al., 2007).

Whole-cell recordings allow for sensitive measures of current density and therefore channel density, but these recordings could be compromised by differences in the intracellular concentration of free calcium and changes to channel biophysics (e.g., conductance and maximum open probability). We confirmed the retention of the chick ortholog of $\alpha_{X7}(60)$ using excised membrane patches where intracellular calcium could be tightly controlled. In this study, $\alpha_{X7}(7)$ and $\alpha_{X7}(60)$ were heterologously expressed in HEK293 cells. The expression vectors were identical except for the C-terminus variations. As a result, transfection efficiency was similar for both plasmids. Pipettes were pulled from a single lot of capillary glass under identical heating conditions to ensure that tip geometry was constant. Consequently, there were no systematic differences in pipette resistance, seal quality, or membrane invagination into the pipette, minimizing differences in channel density due to patch size alone. Steady-state currents were reduced in patches excised from cells transfected with $\alpha_{X7}(60)$ compared to those with $\alpha_{X7}(7)$ (Fig. 4A,B). This difference in current level was reflected in a diminished maximum conductance in patches with $\alpha_{X7}(60)$, only 17% of that in patches with $\alpha_{X7}(7)$ (Fig. 4C). Half-activation voltage was identical between the two constructs (Fig. 4D), suggesting that gating is unaffected by the differences in C-terminus variations. Low-density patches confirmed that single-channel conductance and maximum open probability were also similar between these two constructs (data not shown), leading to the conclusion that differences in maximum conductance were due to alterations in surface expression.

Previous immunocytochemistry studies in our laboratory demonstrated that the acquisition of BK current coincides with trafficking and scaffolding of α subunits in the hair cell basolateral membrane (Li et al., 2009). However, antibodies used in that study were unable to distinguish between C-terminus splice variants. In the following study, we used custom antibodies to determine whether plasmalemmal BK clusters consisted of $\alpha_{X7}(60)$ (anti-VEDEC) or $\alpha_{X7}(7)$ (anti-QEERL). The specificity of these antibodies has been confirmed with Western blot and immunocytochemistry using native tissues and heterologous expression of mammalian BK isoforms (Kim et al., 2007). We further confirmed their specificity for chick isoforms using immunocytochemistry on cloned channels (Supporting Fig. 2).

Confocal analysis of tall hair cells isolated from chick cochlea showed intracellular labeling of the retentive isoform $\alpha_{X7}(60)$ (Supporting Fig. 2D and Supporting Movie S1). The nucleus and intracellular structures dense with cytoskeletal proteins (e.g., the cuticular plate and hair bundle) were notably immunonegative, supporting the conclusion that the label was cytoplasmic. However, the signal did not appear specific to any particular intracellular organelle. The diffuse intracellular labeling with anti-VEDEC was similar to that in chick ciliary ganglion (Kim et al., 2007) and mouse podocytes (Kim et al., 2008). In contrast, anti-QEERL staining was punctate, labeling clusters in the basolateral surface of isolated hair cells (Supporting Fig. 2I and Supporting Movie S2). The labeling profile was similar to that obtained with a commercial BK antibody that targets a nonvariant-specific epitope (Li et al., 2009), revealing one to five distinct, subnuclear puncta in most posthatch tall hair cells. Therefore, $\alpha_{X7}(7)$, and perhaps $\alpha_{X7}(6)$, are the major contributors of BK current in sensory hair cells.

A recent report from our laboratory has shown that anti-BK plaques appear at E18 coincident with the acquisition of calcium-sensitive BK currents (Li et al., 2009). These data also indicated a translocation of these plaques from supranuclear membrane regions (i.e., apicolateral membrane) at E18 to subnuclear regions by E20. Anti-VEDEC and anti-QEERL antibodies were tested on tall hair cells isolated from E15, E18, and posthatch chicks. Anti-QEERL clusters were detected in most cells from E18 onward (Fig. 5A–C), whereas anti-VEDEC staining was diffuse throughout development (Fig. 5D–F). Noprimary controls

were immunonegative at all ages (Fig. 5G–I). Examples of supranuclear and subnuclear anti-QEERL puncta could be found at E18, so we quantified the difference in location of these puncta across these age groups to determine whether BK plaques translocate to basolateral regions as the cell matures. Only cells that were fully isolated and devoid of debris were included in the analysis. No E12 cells exhibited anti-QEERL plaques (data not shown). In the older age groups, the percentage of cells exhibiting puncta steadily increased from E15 to PH, but there was a marked transition in location toward the base of the cell after E18 (Fig. 5J). These data indicate that the acquisition of BK current is well-timed to the developmental appearance of $\alpha_{X7}(7)$ clusters and further supports prior observations of plaque translocation using a different BK α antibody (Li et al., 2009). Transcripts for this variant are present at E12 and expression levels remained stable throughout papillary maturation (Fig. 3B). Therefore, the mechanism underlying the sudden appearance of BK currents in hair cells most likely involves the coordinated synthesis of subunits ending in QEDRL, trafficking of these subunits to the membrane, and scaffolding into basolateral plaques.

DISCUSSION

Early stages of auditory processing encode the intensity, frequency, and temporal aspects of complex sounds, each of which is key for hearing percepts like pitch and speech (Moore, 2008). There is a growing appreciation for the mechanisms that allow hair cells to preserve temporal acuity (Moser et al., 2006). One important contributor is the fast-activating BK current that appears at the onset of hearing in both mammals and nonmammals (Fuchs and Sokolowski, 1990; Marcotti et al., 2003; Pyott et al., 2004; Hafidi et al., 2005). The acquisition of this current transforms immature spiking hair cells into mature sensory receptors. Furthermore, the rapid activation kinetics in these channels shortens the hair cell's membrane time constant, allowing the receptor potential to follow the cycle-by-cycle oscillations of an acoustic stimulus up to several kilohertz. For this reason, the structure–function mechanisms underlying BK channel function are of considerable interest. In this study we sought to determine whether transcription, translation, or trafficking/scaffolding events were correlated with the delayed acquisition of BK currents during hair cell maturation. Similar to another recent report (Li et al., 2009), our results indicated a steady upregulation of BK α transcripts from E12, shortly after hair cell differentiation in chick, to E18, when BK currents appear. The modest 3-fold increase in mRNA levels during this time indicates that transcriptional regulation alone cannot account for the sudden appearance of calcium-sensitive current at the onset of hearing. Our results also indicated that transcriptional control of splicing cannot explain the rapid onset of BK function. Changes in transcript levels do not necessarily correspond to changes in protein levels, and this appears to be the case in our study. A large number of events, each regulated by separate mechanisms, could contribute to the apparent discrepancies between mRNA and protein levels. The efficiency of protein translation, protein stability, multimeric assembly, and trafficking could each contribute to the onset of BK function. Immunofluorescence data indicated a striking change in surface expression of a subpopulation of BK isoforms, suggesting that posttranscriptional trafficking of a distinct pool of BK variants regulates plasma membrane excitability.

The gene expression data also indicated that the relative proportion of alternative exons is, for the most part, established early in hair cell differentiation prior to BK function. Each alternative exon detailed in Fig. 1 is considered below by first describing known or putative roles for the exon in BK biophysics followed by a brief discussion of our results in the context of various model systems.

The 8-amino-acid insert at X1 is the only variant that resides in an extracellular domain. Although a functional role for this variant is unknown, the extracellular position and the presence of a serine phosphorylation motif (Rosenblatt et al., 1997) suggest a possible role in extracellular ATP signaling. Expression has been found in rat brain and trigeminal ganglion (Poulsen et al., 2009) as well as chick cochlea (Rosenblatt et al., 1997). Notably, similar proportions of $\alpha_{X1}(8)$ were found in chick brain and skeletal muscle, suggesting a neuromuscular-specific expression. In contrast, the variant was undetectable in cochlear cDNA from mouse or rat (Langer et al., 2003; Beisel et al., 2007) and was poorly detectable in chick basilar papilla and whole chick cochlea in this study. These data indicate that this exon plays a minimal role, if any, in cochlear BK function. Further study is required to determine the specific function of this variant and whether long-lived proteins might influence hair cell physiology.

The 31-amino-acid insert at X2 is located at the beginning of the RCK1 domain, which plays a critical role in Ca^{2+} sensing and Ca^{2+}-dependent gating (Schreiber and Salkoff, 1997; Xia et al., 2002). Additionally, this site is adjacent to a ring of glutamate residues that have been implicated in setting the large single-channel conductance associated with BK channels (Brelidze et al., 2003; Soom et al., 2008). Studies in fly, mouse, and human have described mutually exclusive splicing of one of several exon repeats at this site (Lagrutta et al., 1994; Soom et al., 2008). Sequence variations among these repeats lead to changes in single-channel conductance, calcium affinity, and voltage-dependent gating (Lagrutta et al., 1994; Soom et al., 2008). Interestingly, splicing at this site in chick and rat cochlea results in a tandem repeat rather than mutually exclusive use of the alternative exons (Navaratnam et al., 1997; Langer et al., 2003). In these cases, the upstream repeat is constitutively present, and alternative splicing results in a concatenation of two repeats. Although an isoform with this tandem repeat has yet to be functionally characterized, the biophysical impact is expected to include changes to conductance, calcium affinity, and gating. Exon 11 includes additional glutamate residues, opening the possibility that additional charged residues near the channel vestibule would increase single-channel conductance. In the current study the tandem repeat was expressed in all tissue samples, indicating that this method of splicing at X2 is common to a variety of cell types. The variant was undetectable in E12 basilar papilla, but expression increased substantially during development. Therefore, $\alpha_{X2}(31)$ may contribute to the wide range in channel properties that have been reported in chick basilar papilla (Duncan and Fuchs, 2003). Notably, expression of this variant is restricted to mid-apical regions of the basilar papilla (Navaratnam et al., 1997), indicating that this variant may participate in tonotopic gradients of electrical tuning. It will be interesting to determine whether region-specific expression is established prior to the appearance of BK currents.

The next three splice sites, X3–X5, are located between the two RCK domains in the cytoplasmic tail of the BK α subunit. We did not consider alternative splicing at X5 due to uncertainty about the presence of this alternative in nonmammalian vertebrates (Beisel et al., 2007). Jones et al. (1999) examined several inserts at X3 and X4, including naturally occurring combinations in turtle cochlea. In general, larger inserts resulted in slower channels with a more negative activation range. The one exception to this rule was the 4-amino-acid insert at X3 (SRKR). When present alone, SRKR generated faster kinetics and decreased Ca^{2+} sensitivity (Rosenblatt et al., 1997; Ramanathan et al., 1999). Between E12 and E15, $\alpha_{X3}(4+)$ increased more than 10-fold and this higher level persisted in older age groups. On the other hand, $\alpha_{X3}(20)$ remained steady until PH, when it increased 2-fold. SRKR includes a potential serine phosphorylation site (Rosenblatt et al., 1997) and the sequence corresponds to an endoplasmic reticulum retention/retrieval motif (Zerangue et al., 1999). It will be important to further characterize the properties and trafficking of variants incorporating SRKR, alone and in combination with other alternatives.

Inserts at X4 were considered previously (Li et al., 2009). The 58 amino acid insert, commonly referred to as STREX, for STRess-axis related EXon (Xie and McCobb, 1998; Erxleben et al., 2002), is of particular functional significance. Incorporation of this exon is regulated by glucocorticoids, and its presence profoundly increases apparent calcium affinity (Tian et al., 2001b; Chen et al., 2005; MacDonald et al., 2006). Phosphorylation of STREX regulates channel response to protein kinase A (Tian et al., 2001a), providing yet another means for generating functional diversity. A steady, modest increase in the developmental expression of $\alpha_{X4}(58+)$, 2-fold greater in PH animals than E11 embryos, cannot explain the sudden appearance of current at E18–19.

Toward the end of the cytoplasmic tail lies the so-called “calcium bowl,” a series of aspartate residues that act as a Ca^{2+} sensing domain. Splice site X6 is located adjacent to this region. The variant, $\alpha_{X6}(28)$, was relatively brain-specific in our study. Representation in the chick basilar papilla was ≈2,000-fold lower than cerebellum. Likewise, representation in other tissues was at least 100-fold lower than that in cerebellum. Although detectable, the proportional expression of this variant was unchanged throughout development. In rat cochlea, the homologous variant at X6 was only detectable after two rounds of PCR amplification (Langer et al., 2003). Taken together, these data suggest that the functional significance of this isoform in the cochlea is minimal.

In chick cochlea, three alternatives have been identified at the C-terminus (Fettiplace and Fuchs, 1999). $\alpha_{X7}(6)$, $\alpha_{X7}(7)$, and $\alpha_{X7}(60)$, ending in sequences EMVYR, QEDRL, and VEDEC respectively, were also found in rat cochlea along with three other C-terminal variations (Langer et al., 2003). While variants with these endings show similar biophysical properties, differences arise in channel trafficking (Kim et al., 2007; Ma et al., 2007) and regulation by microRNAs (Pietrzykowski et al., 2008). Of the three, $\alpha_{X7}(60)$ is retained intracellularly, possibly in mitochondria (Kathiresan et al., 2009). Interestingly, the proportional representation of this variant was comparable in brain and cochlea but reduced in other tissues studied. In basilar papilla, $\alpha_{X7}(60)$ increased between E12 and E15, prior to the onset of BK currents in hair cells. This finding was contrary to our hypothesis that a switch from retentive to nonretentive variants facilitated the advent of BK currents. However, surface expression can be stimulated by chaperones and other factors (Kim et al., 2007, 2008), providing a posttranscriptional molecular switch for modifying channel density in the plasma membrane. If chaperone expression were the rate-limiting step, we would expect an intracellular pool of BK subunits in discrete subcellular organelles. Based on our data, chaperone expression does not appear to be the key regulatory event in hair cell BK development since antibody to the $\alpha_{X7}(60)$ subunit gave diffuse cytoplasmic labeling throughout late-stage maturation.

This work suggests that clusters of $\alpha_{X7}(7)$ and perhaps $\alpha_{X7}(6)$ at the basolateral surface of hair cells are responsible for the appearance of BK currents. The molecular switch leading to the expression of functional $\alpha_{X7}(7)$ at the membrane has yet to be discovered. It is possible that $\alpha_{X7}(7)$ subunits are synthesized early in development and only later assembled and transported to membrane plaques. However, intracellular pools of $\alpha_{X7}(7)$ subunits were not observed, suggesting that mechanisms controlling protein synthesis underlie the delay in acquiring BK currents. Such mechanisms could involve regulators of the initiation, elongation, or termination of BK α translation.

Substantial intracellular labeling with the custom C-terminus antibodies highlights the possibility that hair cell BK channels may be involved in other processes besides electrical tuning. Prior studies have localized BK channels to inner mitochondrial membrane (Siemen et al., 1999), where they play important roles in calcium signaling (Kang et al., 2007). Another recent study identified BK in mitochondrial membrane extracted from whole

cochlear lysates (mouse) and specifically found the trafficking of $\alpha_{X7}(60)$ to mitochondria of CHO cells (Kathiresan et al., 2009). The upregulation of $\alpha_{X7}(60)$ prior to the onset of hearing may be associated with changes in energy demand and mitochondrial calcium signaling rather than requirements for plasmalemmal BK expression and electrical tuning. It will be interesting to determine whether factors known to alter functional BK channel expression in hair cells (e.g., thyroid hormone; Brandt et al., 2007) do so by altering the overall expression of BK isoforms or specifically alter the proportion of variants trafficked to the plasma membrane. These data also underscore the importance of generating a single-gene library of full-length BK transcripts. If upstream inserts specifically and exclusively combine with $\alpha_{X7}(60)$, their effect on hair cell excitability would be minimized, limiting the number of possible isoforms that could contribute to electrical tuning. A full-length library would allow us to predict which alternative exons play a role in shaping the hair cell receptor potential. Some estimates suggest that up to 95% of multiexon genes are subject to alternative splicing (Pan et al., 2008). The chick cochlea provides a fascinating model system for exploring the regulation of multiple splicing events in a single cell type.

Supplementary Material

Refer to Web version on PubMed Central for supplementary material.

Acknowledgments

The authors thank Drs. Mark Crumling and Mingjie Tong for comments on earlier drafts of the article.

Grant sponsor: National Institutes of Health/National Institute on Deafness and Other Communication Disorders (NIH-NIDCD); Grant numbers: R01-DC07432 (to R.K.D.), Core Grant P30-DC05188; Grant sponsor: National Organization for Hearing Research (to R.K.D.).

LITERATURE CITED

Art JJ, Wu YC, Fettiplace R. The calcium-activated potassium channels of turtle hair cells. J Gen Physiol. 1995; 105:49–72. [PubMed: 7730789]

Beisel KW, Rocha-Sanchez SM, Ziegenbein SJ, Morris KA, Kai C, Kawai J, Carninci P, Hayashizaki Y, Davis RL. Diversity of Ca2+-activated K+ channel transcripts in inner ear hair cells. Gene. 2007; 386:11–23. [PubMed: 17097837]

Brandt N, Kuhn S, Munkner S, Braig C, Winter H, Blin N, Vonthein R, Knipper M, Engel J. Thyroid hormone deficiency affects postnatal spiking activity and expression of Ca2+ and K+ channels in rodent inner hair cells. J Neurosci. 2007; 27:3174–3186. [PubMed: 17376979]

Brelidze TI, Niu X, Magleby KL. A ring of eight conserved negatively charged amino acids doubles the conductance of BK channels and prevents inward rectification. Proc Natl Acad Sci U S A. 2003; 100:9017–9022. [PubMed: 12843404]

Chen L, Tian L, MacDonald SH, McClafferty H, Hammond MS, Huibant JM, Ruth P, Knaus HG, Shipston MJ. Functionally diverse complement of large conductance calcium- and voltage-activated potassium channel (BK) alpha-subunits generated from a single site of splicing. J Biol Chem. 2005; 280:33599–33609. [PubMed: 16081418]

Duncan RK. Tamoxifen alters gating of the BK alpha subunit and mediates enhanced interactions with the avian beta subunit. Biochem Pharmacol. 2005; 70:47–58. [PubMed: 15878766]

Duncan RK, Fuchs PA. Variation in large-conductance, calcium-activated potassium channels from hair cells along the chicken basilar papilla. J Physiol. 2003; 547(Pt 2):357–371. [PubMed: 12562934]

Erxleben C, Everhart AL, Romeo C, Florance H, Bauer MB, Alcorta DA, Rossie S, Shipston MJ, Armstrong DL. Interacting effects of N-terminal variation and strex exon splicing on slo potassium channel regulation by calcium, phosphorylation, and oxidation. J Biol Chem. 2002; 277:27045–27052. [PubMed: 12016222]

Fettiplace R, Fuchs PA. Mechanisms of hair cell tuning. Annu Rev Physiol. 1999; 61:809–834. [PubMed: 10099711]

Fodor AA, Aldrich RW. Convergent evolution of alternative splices at domain boundaries of the BK channel. Annu Rev Physiol. 2009; 71:19–36. [PubMed: 18694345]

Fuchs PA, Sokolowski BH. The acquisition during development of Ca-activated potassium currents by cochlear hair cells of the chick. Proc Biol Sci. 1990; 241:122–126. [PubMed: 1978338]

Ha TS, Jeong SY, Cho SW, Jeon H, Roh GS, Choi WS, Park CS. Functional characteristics of two BKCa channel variants differentially expressed in rat brain tissues. Eur J Biochem. 2000; 267:910–918. [PubMed: 10651830]

Hafidi A, Beurg M, Dulon D. Localization and developmental expression of BK channels in mammalian cochlear hair cells. Neuroscience. 2005; 130:475–484. [PubMed: 15664704]

Hamburger V, Hamilton HL. A series of normal stages in the development of the chick embryo. J Morphol. 1951; 88:49–92.

Hille, B. Ion channels of excitable membranes. Sunderland, MA: Sinauer; 2001.

Housley GD, Marcotti W, Navaratnam D, Yamoah EN. Hair cells—beyond the transducer. J Membr Biol. 2006; 209:89–118. [PubMed: 16773496]

Jiang GJ, Zidanic M, Michaels RL, Michael TH, Griguer C, Fuchs PA. CSlo encodes calcium-activated potassium channels in the chick's cochlea. Proc Biol Sci. 1997; 264:731–737. [PubMed: 9178544]

Jones EM, Laus C, Fettiplace R. Identification of Ca(2+)-activated K+ channel splice variants and their distribution in the turtle cochlea. Proc Biol Sci. 1998; 265:685–692. [PubMed: 9608728]

Jones EM, Gray-Keller M, Art JJ, Fettiplace R. The functional role of alternative splicing of Ca(2+)-activated K+ channels in auditory hair cells. Ann N Y Acad Sci. 1999; 868:379–385. [PubMed: 10414307]

Kang SH, Park WS, Kim N, Youm JB, Warda M, Ko JH, Ko EA, Han J. Mitochondrial Ca2+-activated K+ channels more efficiently reduce mitochondrial Ca2+ overload in rat ventricular myocytes. Am J Physiol Heart Circ Physiol. 2007; 293:H307–313. [PubMed: 17351070]

Kathiresan T, Harvey M, Orchard S, Sakai Y, Sokolowski B. A protein interaction network for the large conductance Ca2+-activated K+ channel in the mouse cochlea. Mol Cell Proteomics. 2009; 8:1972–1987. [PubMed: 19423573]

Kim EY, Ridgway LD, Zou S, Chiu YH, Dryer SE. Alternatively spliced C-terminal domains regulate the surface expression of large conductance calcium-activated potassium channels. Neuroscience. 2007; 146:1652–1661. [PubMed: 17478049]

Kim EY, Choi KJ, Dryer SE. Nephrin binds to the COOH terminus of a large-conductance Ca2+-activated K+ channel isoform and regulates its expression on the cell surface. Am J Physiol Renal Physiol. 2008; 295:F235–246. [PubMed: 18480178]

Korovkina VP, Fergus DJ, Holdiman AJ, England SK. Characterization of a novel 132-bp exon of the human maxi-K channel. Am J Physiol Cell Physiol. 2001; 281:C361–367. [PubMed: 11401860]

Lagrutta A, Shen KZ, North RA, Adelman JP. Functional differences among alternatively spliced variants of Slowpoke, a Drosophila calcium-activated potassium channel. J Biol Chem. 1994; 269:20347–20351. [PubMed: 8051129]

Langer P, Grunder S, Rusch A. Expression of Ca2+-activated BK channel mRNA and its splice variants in the rat cochlea. J Comp Neurol. 2003; 455:198–209. [PubMed: 12454985]

Latorre R, Oberhauser A, Labarca P, Alvarez O. Varieties of calcium-activated potassium channels. Annu Rev Physiol. 1989; 51:385–399. [PubMed: 2653189]

Li Y, Atkin GM, Morales MM, Liu LQ, Tong M, Duncan RK. Developmental appearance of BK channels in chick cochlear hair cells. BMC Dev Biol. 2009; 9:67. [PubMed: 20003519]

Livak KJ, Schmittgen TD. Analysis of relative gene expression data using real-time quantitative PCR and the 2(-Delta Delta C(T)) method. Methods. 2001; 25:402–408. [PubMed: 11846609]

Lu R, Alioua A, Kumar Y, Eghbali M, Stefani E, Toro L. Maxi-K channel partners: physiological impact. J Physiol. 2006; 570(Pt 1):65–72. [PubMed: 16239267]

Ma D, Nakata T, Zhang G, Hoshi T, Li M, Shikano S. Differential trafficking of carboxyl isoforms of Ca2+-gated (Slo1) potassium channels. FEBS Lett. 2007; 581:1000–1008. [PubMed: 17303127]

MacDonald SH, Ruth P, Knaus HG, Shipston MJ. Increased large conductance calcium-activated potassium (BK) channel expression accompanied by STREX variant downregulation in the developing mouse CNS. BMC Dev Biol. 2006; 6:37. [PubMed: 16872513]

Marcotti W, Johnson SL, Holley MC, Kros CJ. Developmental changes in the expression of potassium currents of embryonic, neonatal and mature mouse inner hair cells. J Physiol. 2003; 548(Pt 2): 383–400. [PubMed: 12588897]

Moore BC. The role of temporal fine structure processing in pitch perception, masking, and speech perception for normal-hearing and hearing-impaired people. J Assoc Res Otolaryngol. 2008; 9:399–406. [PubMed: 18855069]

Moser T, Neef A, Khimich D. Mechanisms underlying the temporal precision of sound coding at the inner hair cell ribbon synapse. J Physiol. 2006; 576(Pt 1):55–62. [PubMed: 16901948]

Navaratnam DS, Bell TJ, Tu TD, Cohen EL, Oberholtzer JC. Differential distribution of Ca2+-activated K+ channel splice variants among hair cells along the tonotopic axis of the chick cochlea. Neuron. 1997; 19:1077–1085. [PubMed: 9390520]

Oliver D, Taberner AM, Thurm H, Sausbier M, Arntz C, Ruth P, Fakler B, Liberman MC. The role of BKCa channels in electrical signal encoding in the mammalian auditory periphery. J Neurosci. 2006; 26:6181–6189. [PubMed: 16763026]

Pan Q, Shai O, Lee LJ, Frey BJ, Blencowe BJ. Deep surveying of alternative splicing complexity in the human transcriptome by high-throughput sequencing. Nat Genet. 2008; 40:1413–1415. [PubMed: 18978789]

Pietrzykowski AZ, Friesen RM, Martin GE, Puig SI, Nowak CL, Wynne PM, Siegelmann HT, Treistman SN. Posttranscriptional regulation of BK channel splice variant stability by miR-9 underlies neuroadaptation to alcohol. Neuron. 2008; 59:274–287. [PubMed: 18667155]

Poulsen AN, Wulf H, Hay-Schmidt A, Jansen-Olesen I, Olesen J, Klaerke DA. Differential expression of BK channel isoforms and beta-subunits in rat neuro-vascular tissues. Biochim Biophys Acta. 2009; 1788:380–389. [PubMed: 18992709]

Pyott SJ, Glowatzki E, Trimmer JS, Aldrich RW. Extrasynaptic localization of inactivating calcium-activated potassium channels in mouse inner hair cells. J Neurosci. 2004; 24:9469–9474. [PubMed: 15509733]

Ramanathan K, Michael TH, Jiang GJ, Hiel H, Fuchs PA. A molecular mechanism for electrical tuning of cochlear hair cells. Science. 1999; 283:215–217. [PubMed: 9880252]

Ramanathan K, Michael TH, Fuchs PA. beta subunits modulate alternatively spliced, large conductance, calcium-activated potassium channels of avian hair cells. J Neurosci. 2000; 20:1675–1684. [PubMed: 10684869]

Roberts WM, Jacobs RA, Hudspeth AJ. Colocalization of ion channels involved in frequency selectivity and synaptic transmission at presynaptic active zones of hair cells. J Neurosci. 1990; 10:3664–3684. [PubMed: 1700083]

Rosenblatt KP, Sun ZP, Heller S, Hudspeth AJ. Distribution of Ca2+-activated K+ channel isoforms along the tonotopic gradient of the chicken's cochlea. Neuron. 1997; 19:1061–1075. [PubMed: 9390519]

Salkoff L, Butler A, Ferreira G, Santi C, Wei A. High-conductance potassium channels of the SLO family. Nat Rev Neurosci. 2006; 7:921–931. [PubMed: 17115074]

Saunders JC, Coles RB, Gates GR. The development of auditory evoked responses in the cochlea and cochlear nuclei of the chick. Brain Res. 1973; 63:59–74. [PubMed: 4764322]

Schreiber M, Salkoff L. A novel calcium-sensing domain in the BK channel. Biophys J. 1997; 73:1355–1363. [PubMed: 9284303]

Siemen D, Loupatatzis C, Borecky J, Gulbins E, Lang F. Ca2+-activated K channel of the BK-type in the inner mitochondrial membrane of a human glioma cell line. Biochem Biophys Res Commun. 1999; 257:549–554. [PubMed: 10198249]

Soom M, Gessner G, Heuer H, Hoshi T, Heinemann SH. A mutually exclusive alternative exon of slo1 codes for a neuronal BK channel with altered function. Channels (Austin). 2008; 2:278–282. [PubMed: 18719396]

Tian L, Duncan RR, Hammond MS, Coghill LS, Wen H, Rusinova R, Clark AG, Levitan IB, Shipston MJ. Alternative splicing switches potassium channel sensitivity to protein phosphorylation. J Biol Chem. 2001a; 276:7717–7720. [PubMed: 11244090]

Tian L, Hammond MS, Florance H, Antoni FA, Shipston MJ. Alternative splicing determines sensitivity of murine calcium-activated potassium channels to glucocorticoids. J Physiol. 2001b; 537(Pt 1):57–68. [PubMed: 11711561]

Tseng-Crank J, Foster CD, Krause JD, Mertz R, Godinot N, DiChiara TJ, Reinhart PH. Cloning, expression, and distribution of functionally distinct Ca(2+)-activated K+ channel isoforms from human brain. Neuron. 1994; 13:1315–1330. [PubMed: 7993625]

Wong ML, Medrano JF. Real-time PCR for mRNA quantitation. Biotechniques. 2005; 39:75–85. [PubMed: 16060372]

Xia XM, Zeng X, Lingle CJ. Multiple regulatory sites in large-conductance calcium-activated potassium channels. Nature. 2002; 418:880–884. [PubMed: 12192411]

Xie J, McCobb DP. Control of alternative splicing of potassium channels by stress hormones. Science. 1998; 280:443–446. [PubMed: 9545224]

Yu JY, Upadhyaya AB, Atkinson NS. Tissue-specific alternative splicing of BK channel transcripts in Drosophila. Genes Brain Behav. 2006; 5:329–339. [PubMed: 16716202]

Zarei MM, Zhu N, Alioua A, Eghbali M, Stefani E, Toro L. A novel Maxi-K splice variant exhibits dominant-negative properties for surface expression. J Biol Chem. 2001; 276:16232–16239. [PubMed: 11278440]

Zarei MM, Eghbali M, Alioua A, Song M, Knaus HG, Stefani E, Toro L. An endoplasmic reticulum trafficking signal prevents surface expression of a voltage- and Ca2+-activated K+ channel splice variant. Proc Natl Acad Sci U S A. 2004; 101:10072–10077. [PubMed: 15226510]

Zerangue N, Schwappach B, Jan YN, Jan LY. A new ER trafficking signal regulates the subunit stoichiometry of plasma membrane K(ATP) channels. Neuron. 1999; 22:537–548. [PubMed: 10197533]

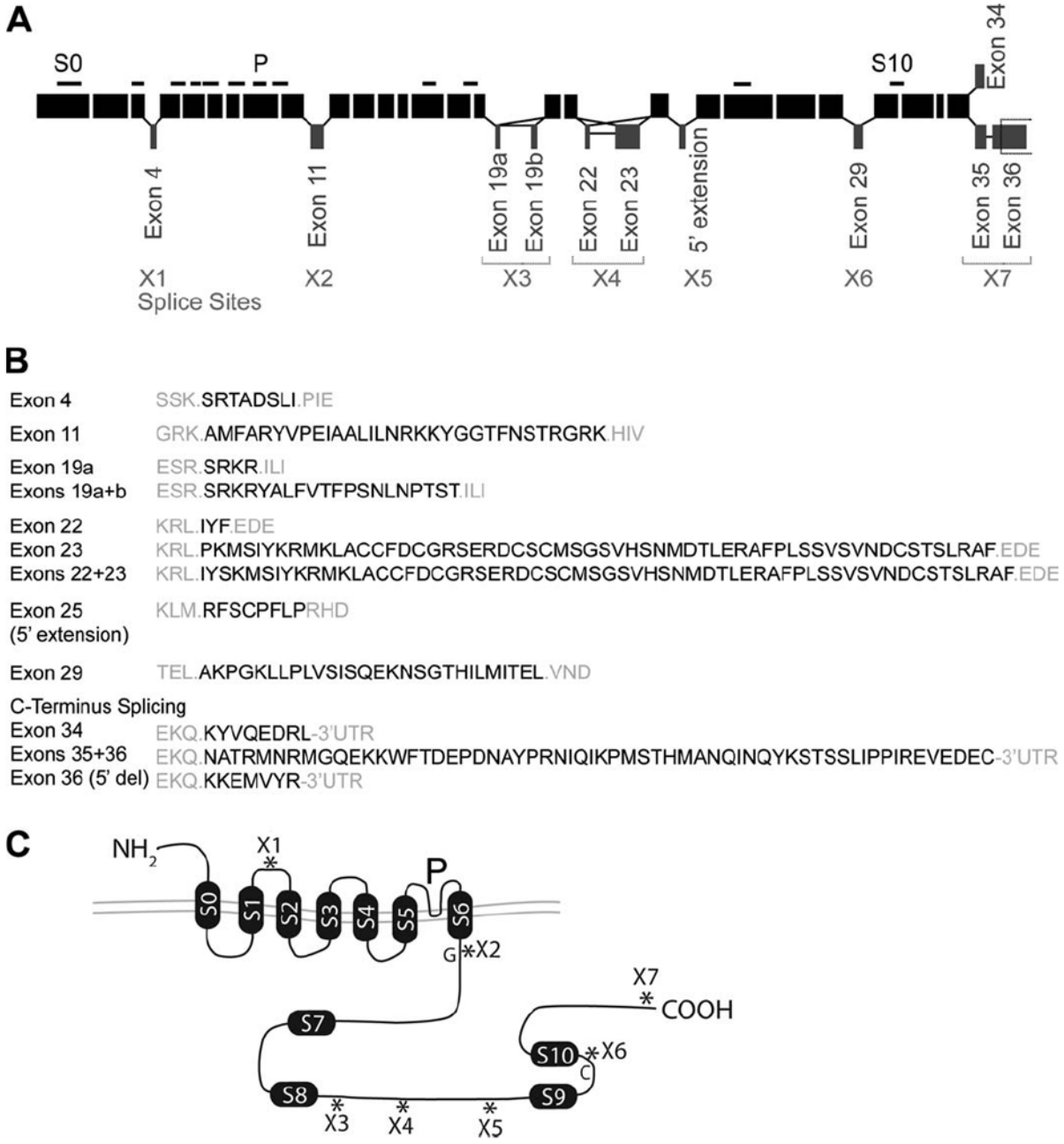

Figure 1.

A: A schematic diagram illustrating the exon structure for chick KCNMA1. Constitutive exons in the short isoform (insertless) are shown as black boxes with relative size corresponding to exon length. Alternatively spliced exons and splice-junction modifications are offset. The number and arrangement of facultative and obligatory exons were derived from online databases (Ensembl ENS-GALT00000007982) and prior reports of splice variant expression in chick cochlea (Navaratnam et al., 1997; Rosenblatt et al., 1997). Splice sites (X1–X7) are marked and numbered according to the scheme of Fettiplace and Fuchs (1999). Variations at the 5′ end of the gene (X0, not shown) have been reported elsewhere (Rosenblatt et al., 1997) but appear to be artifacts (Beisel et al., 2007). Alternative inserts

occur at sites X1, X2, X3, X4, X6, and X7. A 3′ deletion can truncate the alternative exon at X3, giving rise to two possible inserts (exon 19a or exon 19a+b). Two separate alternative inserts at X4 may occur alone or in combination. At X5 a 5′ extension of exon 25 can occur in some species. At X7, mutually exclusive exon use generates several unique C-termini, one consisting of exon 34 ending in the coding sequence QEDRL, one containing exons 35 and 36 and ending in VEDEC, and one incorporating exon 36 with a 5′ deletion resulting in a frameshift ending in EMVYR. The subunit contains 12 hydrophobic domains (horizontal black bars), including seven membrane-spanning regions (S0–S6), four additional soluble hydrophobic domains (S7–S10), and a pore loop (P). **B:** Coding changes are shown for the alternative splicing events illustrated in (A). Gray amino acid residues correspond to flanking obligatory exons and black residues result from splice variation. **C:** The structure of the BK α subunit is shown, relating splice sites to protein topology. The arrangement of transmembrane domains S0–S6 results in an extracellular amino terminus (NH_2) and intracellular carboxy terminus (COOH). Two RCK domains (i.e., regulators of the conductance for potassium) are present, spanning S7 to S8 (RCK1) and S9 to S10 (RCK2). G, glutamate ring essential for the large conductance in BK channels; C, calcium bowl, a high-affinity calcium binding site.

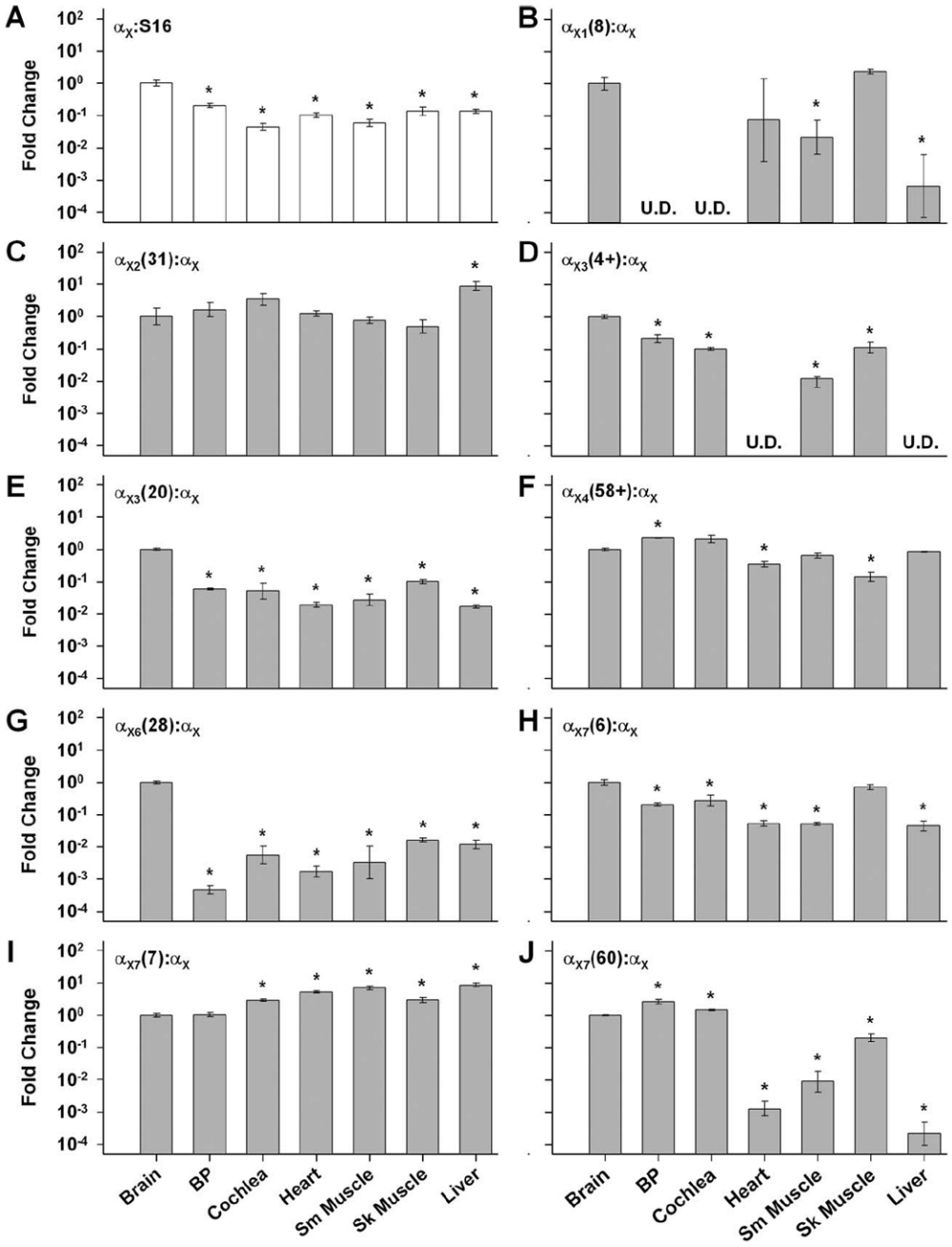

Figure 2.

The tissue distribution of splice variants is shown relative to chick brain (cerebellum). Total RNA from whole tissues was analyzed by qPCR using the TaqMan probes illustrated in Table 1. **A:** Overall expression of BK transcripts was assessed with the nonvariant-specific α_X probe normalized to the housekeeping gene, S16. **B–J:** Variant-specific probes were normalized to α_X in order to determine differences in the representation of that variant among the total pool of transcripts for the tested tissues. U.D. = undetected; $*P < 0.05$.

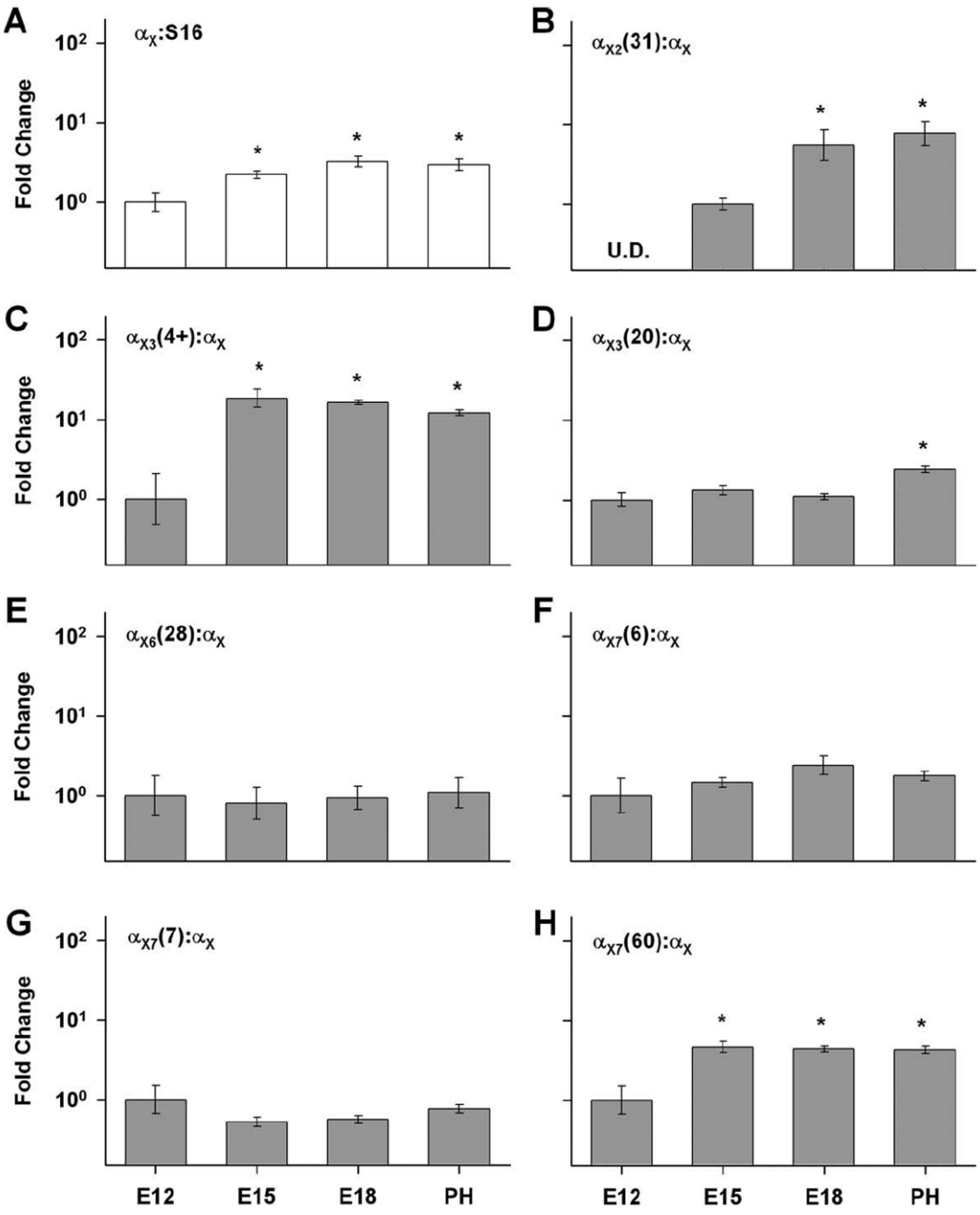

Figure 3.

Developmental changes in BK transcript levels are shown relative to E12. Sensory epithelia from E12, E15, E18, and posthatch animals older than day 5 (PH) were harvested and analyzed with qPCR using the TaqMan probes illustrated in Table 1. **A:** The nonvariant-specific probe α_X was normalized to S16 to assess changes in overall expression levels. BK mRNA increased moderately during development, peaking at E18 near the onset of hearing. **B–H:** Developmental changes in each BK splice variant were measured relative to the total pool of BK transcripts (α_X). Amplification curves for $\alpha_{X1}(8)$ in all samples in all age groups did not reach threshold. Therefore, these data were omitted from the figure. Similarly,

amplification signals for $\alpha_{X2}(31)$ were undetected (U.D.) at E12. In this case, E18 and PH data were normalized to E15 results. $*P < 0.05$.

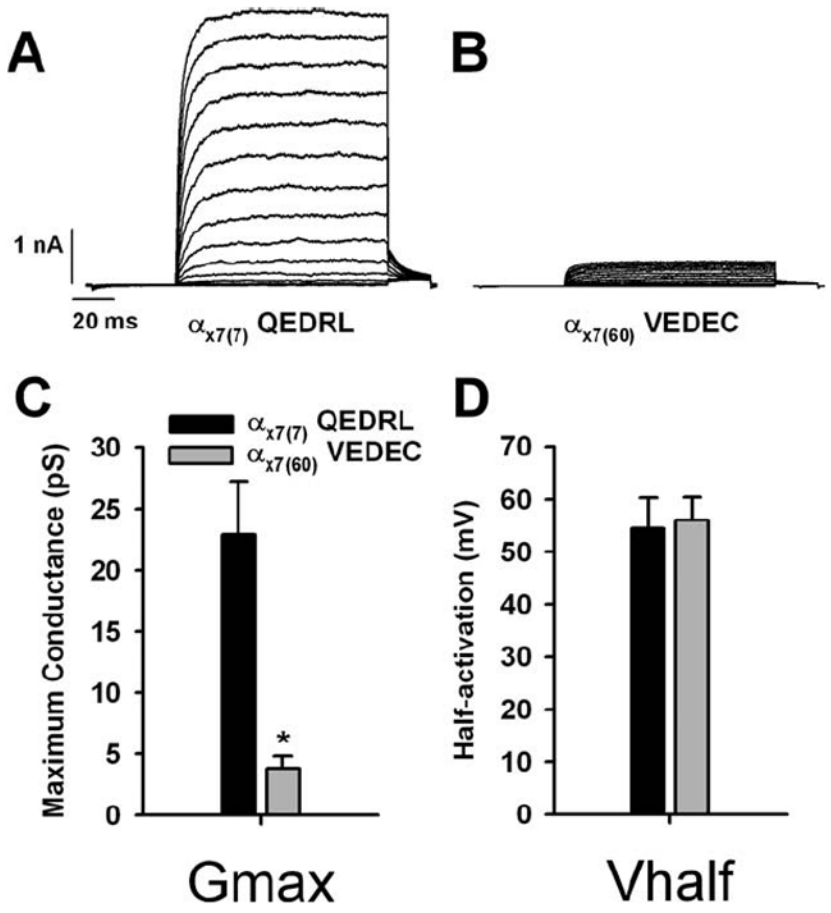

Figure 4.

C-terminus splice variation alters surface expression without changing voltage-dependent gating characteristics. **A,B:** Example current records for inside-out membrane patches are shown. HEK cells were transiently transfected with constructs encoding the $\alpha_{X7}(7)$ (A) or $\alpha_{X7}(60)$ (B) C-terminus variants of the BK α subunit. Plasmid constructs and transfection methods were otherwise identical. Voltage steps ranged from −20 to 130 mV, followed by a step to 20 mV to elicit tail currents. **C:** The maximum conductance produced by the membrane patches was systematically smaller for those cells transfected with $\alpha_{X7}(60)$ compared with $\alpha_{X7}(7)$ (*$P < 0.01$). Single-channel conductance was similar between these two isoforms (data not shown). **D:** Boltzman functions were fit to conductance-voltage curves in order to determine half-activation voltage ($V_{1/2}$). Voltage-dependent gating was unchanged by C-terminal splicing.

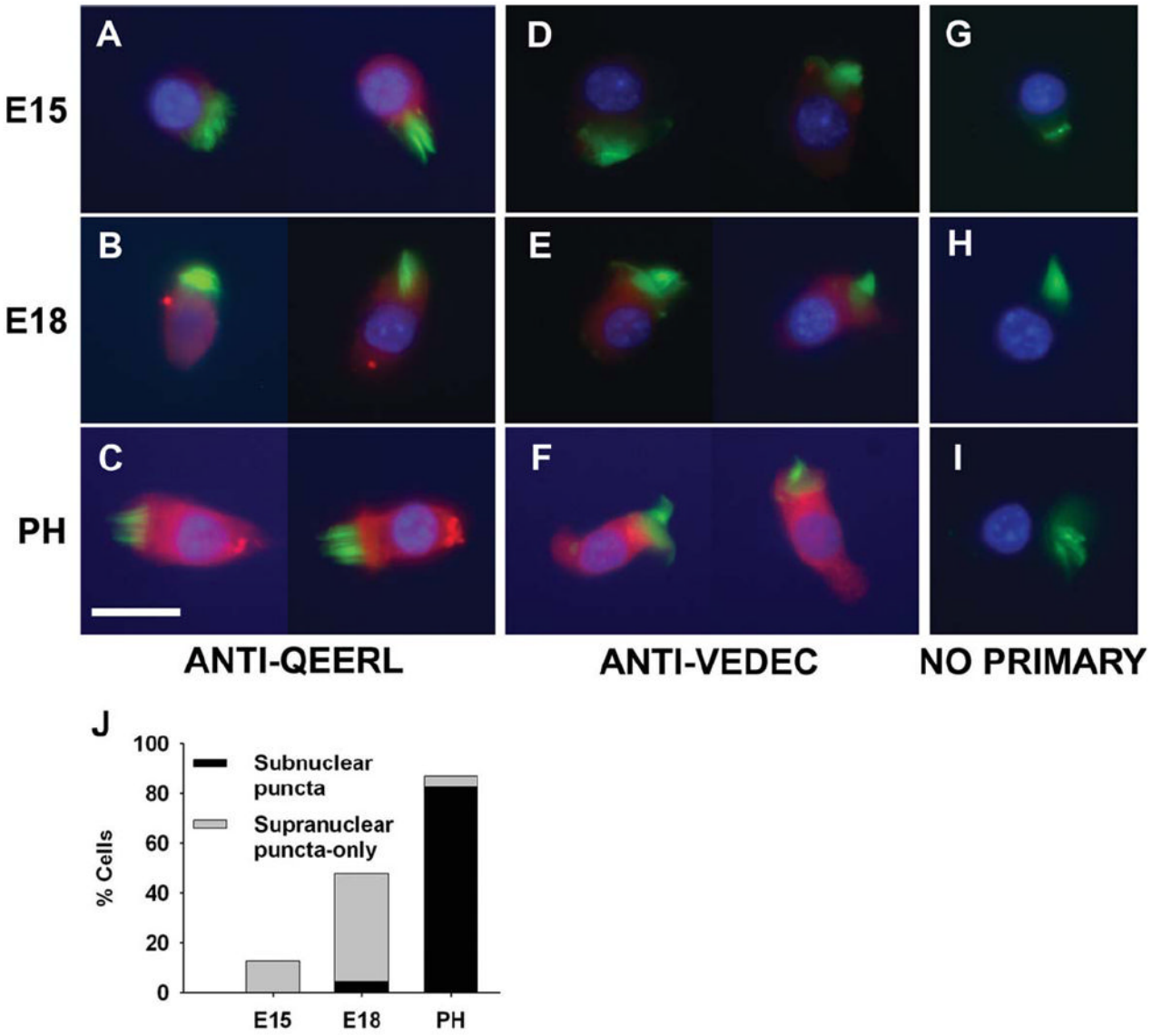

Figure 5.

Immunolocalization of C-terminus variants α_{X7}(60) and α_{X7}(7) during hair cell maturation. Tall hair cells isolated from E15, E18, and PH cochleae were stained with C-terminus specific antibodies (red) as well as markers for the hair bundle (Alexa488-phalloidin, green) and the nucleus (Hoechst counterstain, blue). **A:** Anti-QEERL plaques were absent in hair cells from E15. **B:** By E18 a small number of anti-QEERL puncta could be detected in most cells. **C:** Larger numbers of anti-QEERL puncta were apparent in PH hair cells, and these were typically localized to the basolateral, subnuclear membrane. Hair cells were immunonegative for anti-VEDEC at E15 (**D**), only faintly labeled by E18 (**E**), and diffusely stained with this antibody in posthatch ages (**F**). **G–I:** No-primary controls were immunonegative at all ages. **J:** The percentage of cells with puncta in supranuclear regions (only) and those that exhibited at least some puncta in subnuclear regions were quantified. Scale bar = 10 μm in C (applies to all).

TABLE 1

Primer and Probe Combinations for Real-Time PCR

Target	Alternative exons Involved	Taqman probe sequence	Primers	Primer/ probe map
S16		ACAGGTTCAAGCAGTTTGT	F:AATGATTGAGCCTAGGACTTTGCA	
			R:TCAACACCAGCAAATCTCTCCTT	
α_X Nonvariant-specific		CATGAGCGCAACATAC	F:CAGCGTGCTGGACTCTCT	
			R:CAATGTCCGTATCAGTGTGAGGAT	
α_{X1}(8)	Exon 4	ACGGCTCTTTGATGAATC	F:CGCTCTTAGTATTGGTGCTCTTGTA	
			R:CTGGCAGGATTCTATTGGGATCAA	
α_{X2}(31)	Exon 11	CAAACATTGCCTTTCTTCC	F:GTGGTTCCTATAGTGCGGTTAGT	
			R:GCAGCAATTTCTGGCACGTA	
α_{X3}(4+)	Exon 19a and Exons 19a+b	TTTCGGCTTCTGCTTTCT	F:AATGATAGCCATAGAATACAAGTCGGAAAAA	
			R:TCTTCACATGGTTTCCAGGATTGATC	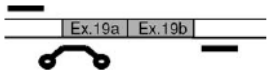
α_{X3}(20)	Exons 19a+b	AAGCGGTATGCCCTCTTC	F:CAAGTCGGAAAAAAGAGAAAGCAGAA	
			R:GGATTGAGGTTGGAAGGAAAGGTAA	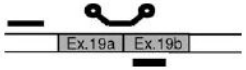
α_{X4}(58+) STREX1/2	Exon 23 and Exons 22+23	TTTACGTGCCTTTGAAGATG	F:CTTCCCACTTTCTTCTGTCTCTGTT	
			R:GTGATAGTGTTGACGGCTGCT	
α_{X6}(28)	Exon 29	TTGCCAGGCTTAGCTAGC	F:CAACAGGAGCCAACATCCCTATTAT	
			R:ACTGATTGAAACCAAAGGCAGAAGT	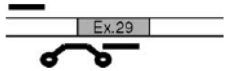
α_{X7}(7) QEDRL	Exon 34	CTTCCTGCACATACTTCT	F:GCACCAAGACCAGGGATTCC	
			R:CACAGTGGGAGCAGATACACATAT	
α_{X7}(6) EMVYR	Exon 36 (5′ deletion)	CCATTTCTTTCTTCTGTTTTTC	F:GCACCAAGACCAGGGATTCC	
			R:GATAGGCATTATCCGGTTCATCTGT	
α_{X7}(60) VEDEC	Exons 35+36	TTGCATTCTGTTTTTCCC	F:GCACCAAGACCAGGGATTCC	
			R:ACCATTTCTTTTCTTGGCCCATTCT